ACS APPLIED MATERIALS & INTERFACES

Research Article

www.acsami.org

Lithium Species in Electrochemically Lithiated and Delithiated Silicon Oxycarbides

Hiroshi Fukui,* Yukinari Harimoto, Masayasu Akasaka, and Katsuya Eguchi

Dow Corning Toray Company, Ltd., Kishi Yamakita, Kanagawa 258-0112, Japan

Supporting Information

ABSTRACT: The work described herein deals with efforts to make a persuasive correlation between structural characteristics and electrochemical lithium storage for a silicon oxycarbide prepared from poly(methylhydrogensiloxane) and divinylbenzene. Structural characterization reveals that the silicon oxycarbide includes excess free carbon in an amorphous network. The reversibility of lithiation and delithiation in the silicon oxycarbide reaches 74% between 0.005 and 3 V relative to lithium at the first cycle but falls to only ca. 30% between 0.4 and 3 V. We found two resonances at 0 and 2.4 ppm in the ^{7}Li magic angle spinning nuclear magnetic resonance spectrum of the silicon oxycarbide lithiated to 0.4 V, whose contributions are 67 and 33%, respectively, and thus are in good agreement with the reversibility observed between 0.4 and 3 V. The fully lithiated silicon oxycarbide shows a single resonance at ca. 3−9 ppm, which tends to broaden at lower temperatures to −120 °C, whereas the fully delithiated silicon oxycarbide has a single resonance at 0 ppm. These results indicate that both reversible and irreversible lithium species have ionic natures. The Li K edge in electron energy loss spectroscopy does not show clearly any identified near-edge fine structures in the inner part of the silicon oxycarbide after delithiation. Near the surface, on the other hand, LiF and oxygen- and phosphorus-containing compounds were found to be the major constituents of a solid electrolyte interface (SEI) layer. Over repeated lithiation and delithiation, the SEI layer appears to become thick, which should in part trigger capacity fading.

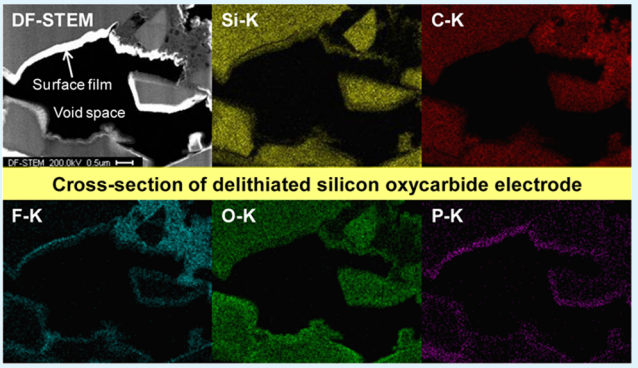

KEYWORDS: *rechargeable lithium batteries, anode material, silicon oxycarbide, amorphous structure, electrochemical lithium storage, lithium species*

INTRODUCTION

Rechargeable lithium-ion batteries have certainly achieved success in consumer applications such as smart phone and lap top computers. In addition, such batteries are steadily filtering into automotive and energy storage applications. Due to increased requirements in battery performance, research efforts need to make further contributions to the advancement of technology. From the perspective of a material, active materials are a prominent figure in rechargeable lithium-ion batteries. Particularly, graphite has been long used as an anode material for several reasons such as operating potential vs lithium and favorable cycling performance. However, graphite is facing its limitation in lithium storage capacity because of the formation of a well-organized stage structure LiC_6 offering a capacity of 372 mA h g^{-1}.[1] Therefore, much effort has been devoted to seeking a high-capacity anode material alternative to graphite. Silicon (Si) simply becomes magnificent in terms of a lithium storage capacity, which is calculated to be ca. 3600 mA h g^{-1} for a metastable phase $Li_{15}Si_4$ based on the weight of Si.[2] A variety of Si-containing materials have also been investigated with ingenuity.[3−5] In a practical sense, in addition to a lithium storage capacity, several factors need to be matched well with the demand for a particular application.

In recent years, silicon oxycarbides and their related materials have drawn renewed attention in the battery research field from electrochemical and materials science standpoints.[6−22] The ability of silicon oxycarbides to electrochemically accommodate lithium ions largely depends on their chemical compositions and structures.[8,18] In general, silicon oxycarbides can be produced from Si-containing polymer precursors through pyrolysis.[23] A wide range of choices for the polymer precursors is highly advantageous, making it possible to tailor the chemical composition of silicon oxycarbides to a reasonable extent. Precisely, pyrolysis conditions,[19,20] such as temperature and processing time, have also significance in determining the characteristics of silicon oxycarbides. Although there are many research reports on silicon oxycarbides as an anode material for rechargeable lithium-ion batteries, one needs to make more robust efforts into deeply understanding their lithium storage

Received: May 7, 2014
Accepted: July 9, 2014
Published: July 25, 2014

mechanism including the initial irreversible capacity loss. Therefore, attempts to identify lithium species stored in silicon oxycarbides still remain a vital task. Because silicon oxycarbides do not typically include Si−Si bonds in a glass network that can be described as xSiC + $(1 - x)$SiO$_2$ (x = 0−1),[24] it would be reasonable to suppose that electrochemical lithium storage in silicon oxycarbides is far different from that in Si. Previous work has shown that lithium species can be stored in more than one site of a silicon oxycarbide prepared from a blend of phenyl-substituted polysilane and polystyrene.[9] There have also been reports that deal with lithium storage mechanisms for different types of silicon oxycarbides.[21,22] It should be underscored that different polymer precursors could form different silicon oxycarbides; a major difficulty may be involved in applying a lithium storage mechanism proposed for one particular silicon oxycarbide to the other.

The morphology and composition of a thin film, generally called a solid electrolyte interface (SEI) layer, on graphite have become focuses of research.[25] Literature reports have shown that lithium compounds, such as LiOH,[26] are major components in the SEI layer. Because the surface state of active materials is not exactly the same, such characteristics of the SEI layer are complex, also depending on type of electrolyte.[27] Unfortunately, to the best of our knowledge, little information is available on the formation of the SEI layer on silicon oxycarbides. Reversible lithiation and delithiation suggests that the SEI layer plays a key role in transporting lithium ions from electrolyte solutions during lithiation and from silicon oxycarbides during delithiation.

In this paper, we discuss electrochemical lithium storage in a silicon oxycarbide derived from poly(methylhydrogensiloxane) (PMHS) and divinylbenzene (DVB). In an attempt to identify lithium species in the interior and the exterior of this particular silicon oxycarbide, several powerful analytical techniques, such as ^{7}Li nuclear magnetic resonance (NMR) and scanning transmission electron microscopy (STEM)/electron energy loss spectroscopy (EELS), have been employed. ^{7}Li NMR analysis provides an average level of information on the local environment of lithium species. On the other hand, STEM/EELS measurements allow us to directly observe the SEI layer as well as the electronic environment of lithium species in a certain area of the silicon oxycarbide. Careful attention is paid here to the silicon oxycarbide to achieve a stringent correlation between structural characteristics and electrochemical lithium storage.

EXPERIMENTAL METHODS

Material Preparation. DVB (Divinylbenzene 570, Nippon Steel Chemical, 775 g) and PMHS (Dow Corning, 531 g) were cross-linked with Karstedt's catalyst at 120 °C in air. The total ratio of silicon hydride to unsaturated group is 1.0 and the total concentration of elemental Pt is 10 ppm. The cured polysiloxane precursor (969 g) was put in an alumina boat and then heat treated in a furnace at 600 °C for 2 h. Highly purified nitrogen was flown at 2 L min^{-1} during heat treatment and the temperature rising rate was 2 °C min^{-1}. 591 g of a char intermediate obtained was placed in an alumina boat and then pyrolyzed at 1000 °C for 1 h under an argon atmosphere. The argon flow rate and the temperature rising rate were 100 mL min^{-1} and 5 °C min^{-1}, respectively. The silicon oxycarbide monolith obtained was finally jet-milled to be particles having a diameter of ca. 10 μm.

Material Analysis. The chemical composition of the silicon oxycarbide was determined by elemental analysis. The CHN analyses were performed on an NCH-22F (Sumika Analytical Service) and a CS-LS600 (Leco). Because the content of N was negligible, we do not discuss it in this paper. The oxygen content was determined using an EMGA-2800 (Horiba). Following a fusion process where a solid sample is turned to be a soluble form, the Si content analysis was carried out with an inductively coupled plasma (ICP) technique (iCAP6500DuoView, Thermo Fisher Scientific). The contents of C, H, O, and Si were 45.7, 0.8, 20.6, and 29.0 wt %, respectively. Solid-state ^{13}C and ^{29}Si magic angle spinning (MAS) nuclear magnetic resonance (NMR) analyses were conducted at 75.2 MHz (CMX-300 Infinity, Chemagnetics) and 59.6 MHz (AC300 spectrometer, Bruker), respectively. The detailed procedure for ^{29}Si MAS NMR analysis has been explained elsewhere.[9] Regarding ^{13}C MAS NMR analysis, dipolar decoupling (DD)/MAS, cross polarization (CP)/MAS, and dipolar dephasing techniques were applied in this study. The signals related to ^{13}C in the silicon oxycarbide had the longitudinal relaxation time, T_1, in the range 1.8−2.8 s. Recycle delays of 50 and 5 s were taken for DD/MAS technique and CP/MAS and dipolar dephasing techniques, respectively, with a pulse width of 4.2 μs (θ = 90°) in common. In addition, electron spin resonance (ESR) measurements were performed at 9.46 GHz using a Bruker ESP350E equipped with a cryostat (ESR910, Oxford). ESR spectra were collected at 10, 20, 40, 80, and 296 K by sweeping the magnetic field (center = 3375.3 G) in a range ±50 G. The radical content of the silicon oxycarbide was determined on the basis of a standard material (ion-doped polyethylene film). Following a focused ion beam (FIB) process (FB-2000A, Hitachi), cross-sectional STEM, high-angle annular dark-field (HADDF)-STEM, and EDX spectroscopy mapping (C, O, and Si) images were captured using a JEM2100F (JEOL) equipped with a JED-2300T (JEOL) for the silicon oxycarbide embedded in an epoxy resin. The corresponding selected area electron diffraction (SAED) pattern was also collected for the same sample specimen.

Electrochemical Testing. Electrochemical lithiation and delithiation of the silicon oxycarbide was performed using a battery cycler (Hokuto Denko, HJ1010mSM8A) at 30 °C. Prior to coin cell fabrication (either 2016- or 2032-type) in an argon-filled glovebox, a working electrode (14 mm diameter) was prepared by mixing the active material, acetylene black, and poly(vinylidene fluoride) (PVDF) in a weight ratio of 85:5:10. The powdery mixture dispersed in *N*-methyl-2-pyrrolidinone (NMP, Wako Pure Chemical Industries) was coated on copper foil. After NMP removal, the working electrode was cut away from the copper foil. Lithium foil (15 mm diameter, Honjo Metal) was used as the counter electrode. The electrolyte used was 1 mol dm^{-3} LiPF$_6$ dissolved in a mixed solution of ethylene carbonate and diethyl carbonate (1:1 by volume, Kishida Chemical). A polymer film was sandwiched between the working electrode and the counter electrode as a separator. Assuming that a theoretical capacity is 700 mA h g^{-1}, electrochemical lithiation was performed at 0.1C under a constant voltage condition until the current reaches a value corresponding to 0.01C, whereas electrochemical delithiation was conducted under the same constant current condition unless otherwise noted. The cutoff voltage was varied between 0 and 3 V for the purpose intended.

Lithiated/Delithiated Sample Analysis. All sample handling was carefully performed under an argon atmosphere or using a specially designed transfer vessel to avoid exposure to open air. For ^{7}Li NMR analysis, coin-type cells were dismantled in the glovebox after reaching a certain depth of lithiation (DOL) and delithiation (DOD), and then the working electrodes at different DOLs and DODs were washed with dimethyl carbonate (Tomiyama Pure Chemical Industries). ^{7}Li NMR spectra were measured on a CMX-300 spectrometer (116.2 MHz, Chemagnetics) at 25 °C. At DOL = 100% ^{7}Li NMR spectra were also collected at low temperatures (0 to −120 °C). Relaxation times, T_1 and T_2, were measured at different temperatures, ranging from ca. 0.5 to 2.4 s and from ca. 0.04 to 0.10 ms, respectively. A recycle delay of 2−12 s was used for single pulse excitation with a pulse width of ∼1.40 μs (θ = 30°) depending on measuring temperatures. The samples were spun at 9−10 kHz if necessary. All ^{7}Li NMR spectra obtained in this study were referenced to LiCl (0 ppm). STEM, HADDF-STEM, and energy-dispersive X-ray (EDX) spectroscopy mapping (C, O, F, Si, and P) images were obtained from thin-film working electrodes in a delithiated state prepared by FIB,

after 2 and 28 cycles, at 200 kV using an HD-2700 (Hitachi High Technologies). EELS spectra were also collected to gather information on local environments of C, O, Si, and Li for the same thin film specimen.

RESULTS

After pyrolysis to 1000 °C under an argon atmosphere and milling, black silicon oxycarbide powders were obtained from a cured form of PHMS and DVB. According to elemental analysis, the silicon oxycarbide was found to have the chemical composition described as $SiO_{1.2}C_{3.7}H_{0.8}$. Because the ratio of C to Si in PHMS is almost 1.1, excess carbon, as seen in the chemical composition, must be supplied by DVB unless Si is removed during the course of pyrolysis. In this regard, our preliminary experiment confirms that major components detected by TGA coupled with GC/MS analyses do not contain Si-containing species.

Figure 1a shows the cross-sectional STEM image of the silicon oxycarbide embedded in an epoxy resin. It can be seen

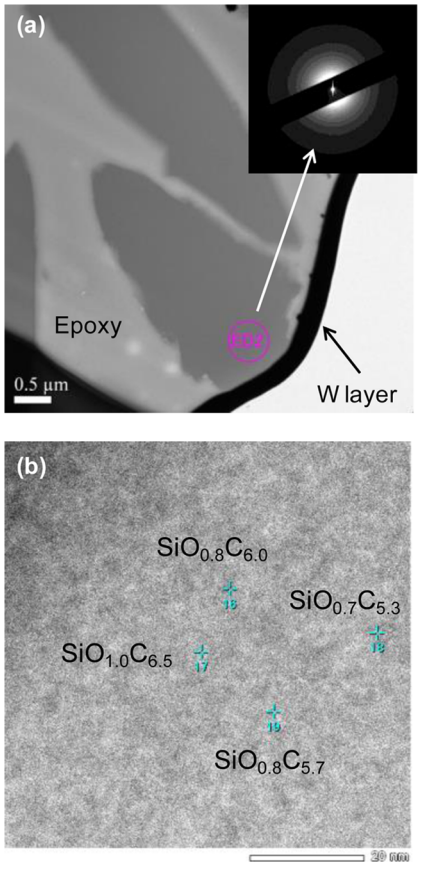

Figure 1. (a) STEM and (b) HADDF-STEM image of a cross section of the silicon oxycarbide embedded in an epoxy resin. The inset in panel 1a represents the corresponding SAED pattern.

that the silicon oxycarbide has particles of irregular shape. The corresponding SAED pattern in the inset of Figure 1a represents the amorphous nature of the silicon oxycarbide with only a diffuse diffraction ring. This is mainly due to the pyrolysis temperature set in this study lower than that leading to the formation of crystalline phases such as silicon carbide.[24] Figure 1b shows the HADDF-STEM image of an inner part of the silicon oxycarbide. The contrast of the image was indistinct partly because of no large difference in atomic number among three elements (C, O, and Si) present in the silicon oxycarbide. It is of interest to analyze how such elements are dispersed in the silicon oxycarbide. EDX analysis shows that at least O and Si are likely to be dispersed throughout each particle of the silicon oxycarbide (Figure S1 in the Supporting Information). We also made an attempt to measure local compositions at four different locations inside the silicon oxycarbide, as indicated in Figure 1b. The local compositions ($SiO_{0.7-1.0}C_{5.3-6.5}$) are in general different from the chemical composition ($SiO_{1.2}C_{3.7}$) determined by elemental analysis but fall within a relatively narrow range at several nanometers scale.

Concerning the local environment of silicon in the silicon oxycarbide, ^{29}Si MAS NMR analysis shows that there are mainly four resonances at ca. −12 (26.52%), −38 (19.69%), −75 (22.91%), and −111 ppm (30.88%) (Figure 2a). These

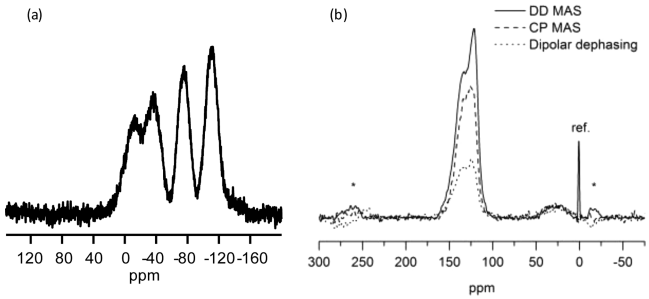

Figure 2. (a) ^{29}Si MAS NMR and (b) ^{13}C DD/MAS, CP/MAS, and dipolar dephasing NMR spectra of the silicon oxycarbide. An asterisk indicates spinning sideband.

resonances may be attributed to local silicon environments usually described as SiC_4, SiC_2O_2, $SiCO_3$, and SiO_4, respectively.[24] We show the ^{13}C DD/MAS, CP/MAS, and dipolar dephasing NMR spectra of the silicon oxycarbide in Figure 2b. The ^{13}C NMR resonances were grouped into two; the minor broad resonance at 10−40 ppm and the major broad resonance at 110−160 ppm. The dipolar dephasing technique is sensitive to both aliphatic carbon CH_3 and quaternary carbon,[28] whereas the CP/MAS technique enhances the sensitivity of dilute ^{13}C spins by the neighboring abundant ^{1}H spins.[29] We observed that there was little enhancement of the 10−40 ppm resonance by the CP/MAS technique but rather a slight enhancement by the dipolar dephasing technique. Therefore, the 10−40 ppm resonance may be mainly associated with quaternary carbon bound to silicon (C−Si)[30] rather than aliphatic carbon such as CH_3. In general, the resonances associated with aromatic carbon can be seen in the range 90−165 ppm.[31] The 110−160 ppm resonance observed for the silicon oxycarbide was mainly related to aromatic carbon bound to hydrogen or carbon.[31] The relative intensity of the resonance at ca. 123 ppm became weak by the CP/MAS technique. Therefore, the 110−160 ppm resonance is probably derived from aromatic carbon bound to carbon but not hydrogen. Given that no resonance was observed at 170−200 ppm, both COOR (R = H, alkyl, etc.) and CO groups were not identified.[31] Comparison between the 10−40 ppm and the 110−160 ppm resonance confirms that the silicon oxycarbide has excess carbon called free carbon as a major constituent, which is usually inseparable in this type of material.[24]

Figure 3a shows the first-derivative ESR spectrum of the silicon oxycarbide obtained at 296 K. A single signal was observed at ca. 3376 G (g = 2.0023). The spin density of the

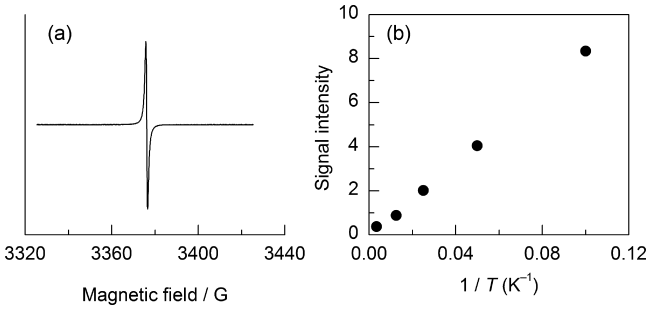

Figure 3. (a) First-derivative ESR spectrum of the silicon oxycarbide obtained at 296 K and (b) temperature (T) dependence of ESR signal intensities.

silicon oxycarbide was estimated to be 3.8×10^{19} spins g^{-1}. The g-value can be attributable to radicals present on carbon but not silicon in the silicon oxycarbide.[32] It is known that a temperature-dependent ESR signal intensity provides further insights into type of radical; either localized or conduction electrons. As shown in Figure 3b, the signal intensity crosses the origin, directly proportional to the reciprocal of temperatures ranging from 10 to 296 K. In addition, the ESR line width tended to broaden as temperatures decreased. These results indicate that the radicals observed for the silicon oxycarbide are basically localized paramagnetic centers on carbon.[33]

Figure 4 shows the lithiation and delithiation curve of the silicon oxycarbide obtained at the first cycle. In the inset of

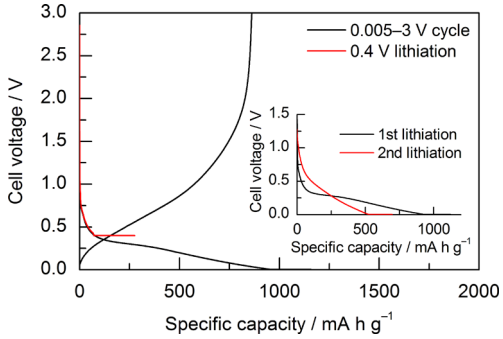

Figure 4. Lithiation and delithiation curves of the silicon oxycarbide obtained at the first cycle. The inset shows a typical difference in lithiation curve between the first and the second cycle.

Figure 4, a comparison between the first and the second lithiation curve is also shown. In the voltage range 0.005−3 V, the silicon oxycarbide had a lithiation capacity of 1159 mA h g^{-1} and a delithiation capacity of 862 mA h g^{-1}, leading to a Coulombic efficiency of 74%. The silicon oxycarbide features an obvious voltage hysteresis between lithiation and delithiation curves. It has been reported that the gap in cell voltage observed for a silicon oxycarbide persists even after sufficient relaxation times.[34] Thus, it is suggested that there is a different electrochemical equilibrium between lithiation and delithiation reactions. In Figure 4, we also show the first-cycle lithiation curve of the silicon oxycarbide to 0.4 V. Because the silicon oxycarbide has a Coulombic efficiency of ca. 30% between 0.4 and 3 V, a majority of the capacity (276 mA h g^{-1}) observed during lithiation to 0.4 V becomes irreversible.

Figure 5 shows the room-temperature ^{7}Li MAS NMR spectra of the silicon oxycarbide cycled between 0.005 and 3 V,

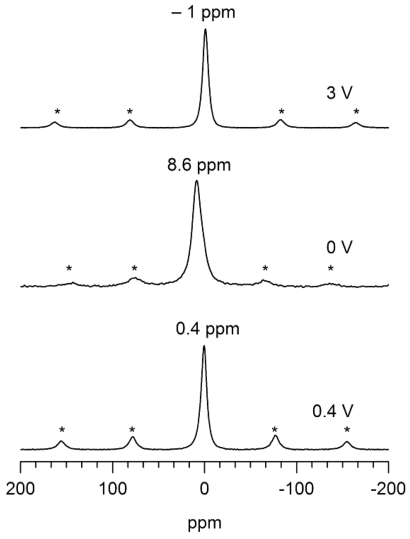

Figure 5. Room-temperature ^{7}Li MAS NMR spectra of the silicon oxycarbide cycled between 0.005 and 3 V, lithiated to 0 V and short circuited, and partially lithiated to 0.4 V. An asterisk indicates spinning sideband.

lithiated to 0 V and short circuited, and partially lithiated to 0.4 V. All spectra exhibit at least one resonance near 0 ppm. Of particular interest is the similarity between the silicon oxycarbide cycled between 0.005 and 3 V and the silicon oxycarbide partially lithiated to 0.4 V. Both silicon oxycarbides show a resonance at almost 0 ppm, which is indicative of a more ionic nature of lithium species than that formed in the fully lithiated silicon oxycarbide; the lithium species responsible for the initial irreversible capacity apparently have an ionic nature such as LiCl used as a reference. As mentioned above, irreversible reactions account for 70% of the total amount of lithium species stored between 0.4 and 3 V; the rest of the lithium species (30%) can only be used in a reversible manner. We further analyzed the ^{7}Li NMR spectrum measured for the silicon oxycarbide partially lithiated to 0.4 V, as shown in Figure 6. The 0.4 ppm resonance can be separated into two resonances; one is centered at 2.4 ppm and the other is centered at 0 ppm. The 2.4 ppm and the 0 ppm resonance have a contribution of 33% and 67%, respectively.

It has been reported that lithium species stored in anode materials, such as hard carbon, feature mobility, which appears as a resonance shift in NMR spectra at lower temperatures.[35,36]

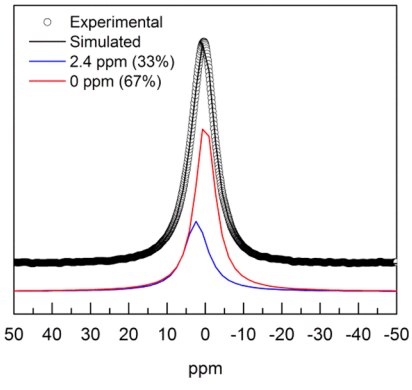

Figure 6. Experimental and simulated ^{7}Li MAS NMR spectra of the silicon oxycarbide partially lithiated to 0.4 V.

In this study, we directed our attention to how measuring temperatures affect ^{7}Li NMR resonances. Figure 7 shows the

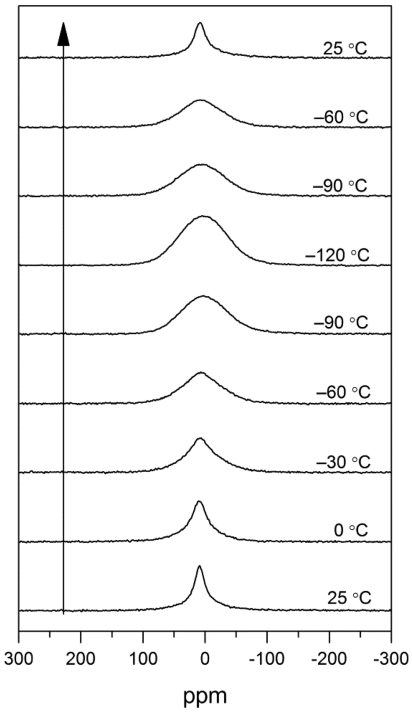

Figure 7. ^{7}Li NMR spectra of the fully lithiated silicon oxycarbide measured in the temperature range +25 to −120 °C.

static ^{7}Li NMR spectra for the fully lithiated silicon oxycarbide measured in the temperature range +25 to −120 °C. One noticeable change is that the peak shape tends to broaden as measuring temperatures become lower. Even at −120 °C, there appears to be no clear peak separation, as opposed to the case of a silicon oxycarbide previously reported[9] and hard carbon.[35,36] In Figure 8, we show a plot of ^{7}Li NMR resonances

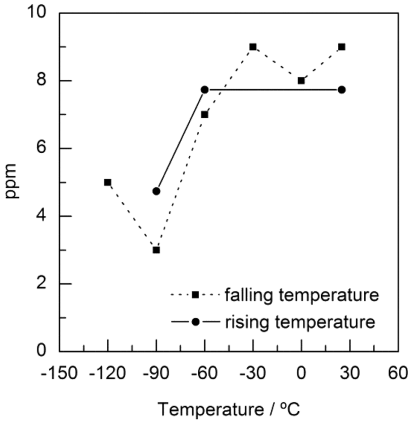

Figure 8. Relationship between ^{7}Li NMR resonances and measuring temperatures for the fully lithiated silicon oxycarbide.

vs temperatures. Interestingly, the ^{7}Li NMR resonances were shifted within a very narrow range ca. 3−9 ppm between falling and rising temperature directions.

A further attempt was made to achieve a better understanding of how lithium species remain in the interior and exterior of the silicon oxycarbide. The delithiated silicon oxycarbide was analyzed after 2 and 28 cycles between 0.005 and 1.5 V using STEM/EDX techniques. The cross-sectional STEM and the corresponding EDX mapping images of the working electrode after 2 cycles are shown in Figure 9. The

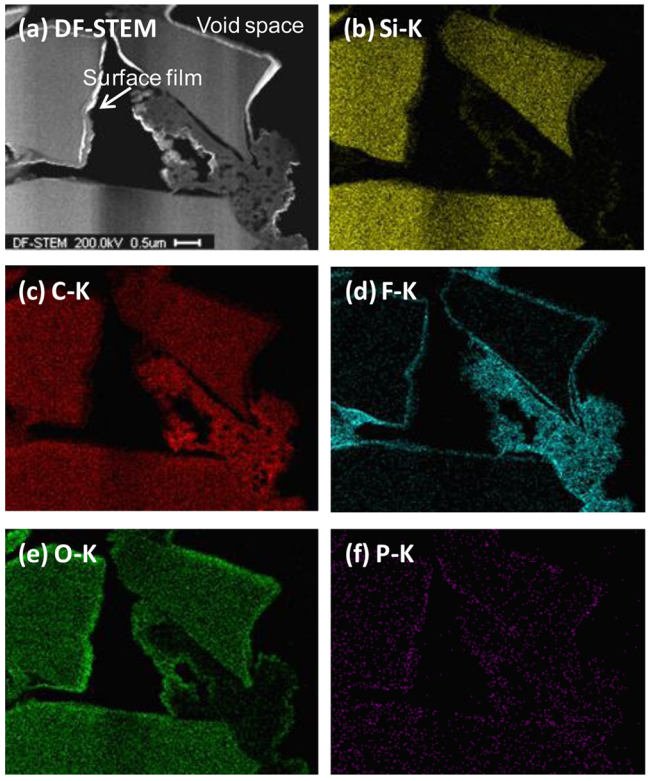

Figure 9. (a) Cross-sectional STEM image and (b−f) the corresponding EDX mapping images (Si, C, F, O, and P) of a silicon oxycarbide composite electrode in a delithiated state after 2 cycles. Electrochemical lithiation and delithiation rates were 0.5 and 0.1C, respectively, at the second cycle.

STEM image in Figure 9a and the Si map in Figure 9b confirm that the cycled electrode still has silicon oxycarbide particles of irregular shape with some void spaces and that the particles do not fracture over 2 cycles. Because all components include carbon as a constituent element, the C map in Figure 9c does not reflect a different level of distribution in the whole region except the void spaces. PVDF is located between the silicon oxycarbide particles, apparently forming aggregates based on the F map in Figure 9d. In addition, it clearly indicates that F-containing compounds are present near the surface of the silicon oxycarbide particles. The O map in Figure 9e shows that O is an element near the edge of the PVDF aggregates somehow as well as in the silicon oxycarbide particles. This might be due to the presence of very small silicon oxycarbide particles trapped in PVDF. In addition, there could also exist some O-containing compounds formed on the surface of the silicon oxycarbide. According to the P map in Figure 9f, it can be seen that P-containing compounds are also formed on the surface of the silicon oxycarbide particles. Figure 10a,b shows the HAADF-STEM image and EELS (Li K edge) spectra for the working electrode after 2 cycles. We analyzed in total 20 different points from the interior to the exterior in a delithiated silicon oxycarbide particle but show only five representative points (1, 6, 11, 16, and 20 in Figure 10a). There was little difference in the EELS spectra of Li K edge from the interior to

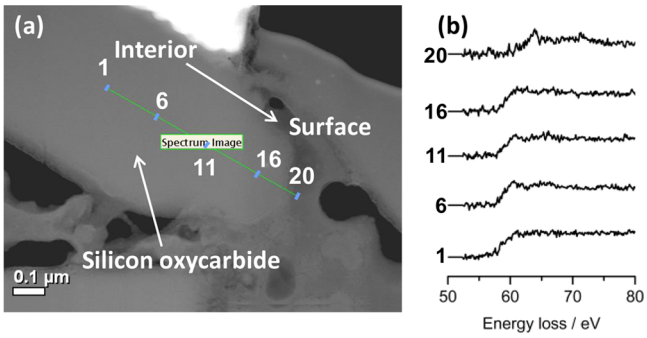

Figure 10. (a) HAADF-STEM image and (b) EELS Li K edge spectra of a silicon oxycarbide composite electrode in a delithiated state after 2 cycles.

the exterior of the silicon oxycarbide particle after 2 cycles. However, interestingly, a different Li K edge spectrum (point 20 in Figure 10b) was obtained near the surface of the particle where no Si was indentified (Figure S2 in the Supporting Information).

The same set of experiments was performed for the working electrode after 28 cycles. Figure 11 shows the cross-sectional

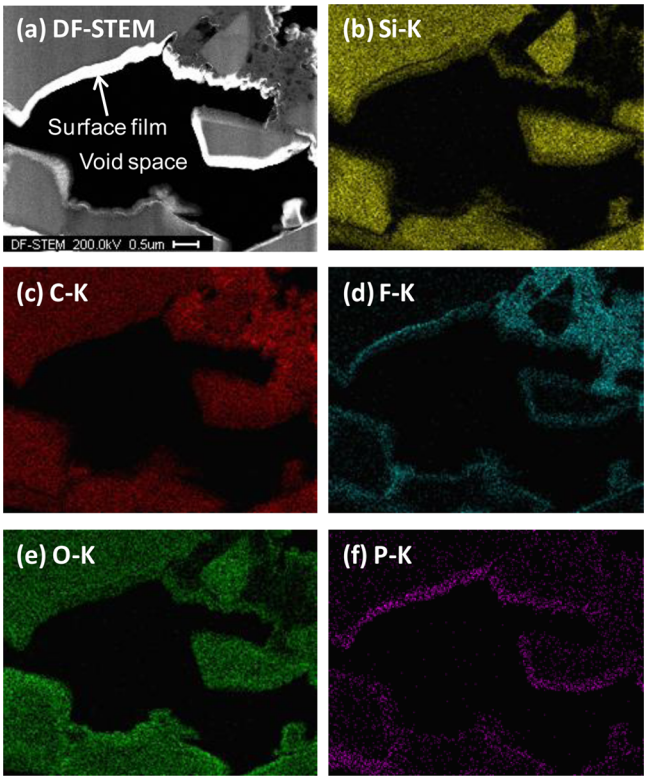

Figure 11. (a) Cross-sectional STEM image and (b–f) the corresponding EDX mapping images (Si, C, F, O, and P) of a silicon oxycarbide composite electrode in a delithiated state after 28 cycles. Both electrochemical lithiation and delithiation rates were 0.2C between the second cycle and the 27th cycle.

STEM and the corresponding EDX mapping images of the cycled working electrode. The silicon oxycarbide particles appear to remain intact even after 28 cycles (Figure 11a). As a whole, the results show five-element maps almost similar to those obtained from the electrode after 2 cycles (Figure 11b–f). As seen in the case of the electrode after 2 cycles, a significant change in Li K edge spectrum was observed near the surface of the silicon oxycarbide particle after 28 cycles (points 16 and 20 in Figure 12a,b). The repeated lithiation and

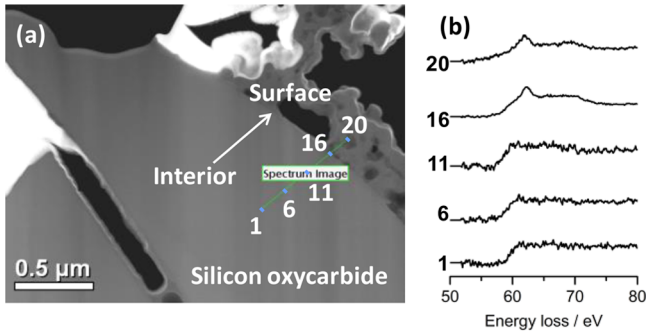

Figure 12. (a) HAADF-STEM image and (b) EELS Li K edge spectra of a silicon oxycarbide composite electrode in a delithiated state after 28 cycles.

delithiation provides a clear Li K edge spectrum showing a peak at ca. 62.5 eV. According to the feature of the spectrum, LiF appears to be formed near the particle surface.[37] We have confirmed that the surface regions where LiF is found hardly include detectable Si (Figure S3 in the Supporting Information). We notice that LiF tends to grow over such a longer cycle as well as O- and P-containing compounds (Figure 11d).

DISCUSSION

Composition and Structural Characteristics. As seen in the STEM-EDX measurements, it appears that the composition of the silicon oxycarbide is relatively homogeneous in the amorphous network evidenced by SAED analysis. DVB has been reported to increase the content of free carbon in silicon oxycarbides through thermal decomposition.[38] Based on the stoichiometric description of $SiC_xO_{2(1-x)}$,[24] our elemental analysis shows that the silicon oxycarbide consists of excess free carbon yC; $SiC_{0.4}O_{1.2}$ + 3.3C. The ^{13}C NMR experiments also support the idea that the silicon oxycarbide includes a free carbon phase. Because quantitative analysis is possible by measuring the ^{13}C NMR spectra in full consideration of T_1 (=1.8–2.8 s) for the resonances observed, free carbon can be excess in the silicon oxycarbide. In the lower field 110–160 ppm, at least two major resonances are identified, which can typically be assigned to aromatic carbon. Various types of aromatic carbon could be present in the silicon oxycarbide. We see that the silicon oxycarbide has little hydrogen bound to aromatic carbon by comparison between the DD/MAS, CP/MAS, and dipolar dephasing experiments. As stated above, elemental analysis shows that a non-negligible amount of hydrogen is present in the silicon oxycarbide. Due to the broadening of the 10–40 ppm peak in the ^{13}C NMR spectra (Figure 2b), we cannot completely rule out the possibility that hydrogen is present in aliphatic carbon. Given that our pyrolysis temperature is 1000 °C, free carbon can have disordered structures with some groups (e.g., C–OH) on the edges, which can be observed at 150–165 ppm.[31]

Although there could be uncertainty because of a large distribution of local silicon environments and some peak overlaps, a silicon oxycarbide phase can be identified by ^{29}Si MAS NMR analysis on some level. The four distinguishable resonances indicate that the silicon oxycarbide phase is basically

made up of Si−C and Si−O bonds. In this study, because the precursor was pyrolyzed at 1000 °C, it is possible that redistribution of such Si−C and Si−O bonds occurs during the course of decomposition as previously reported.[23] Assuming that quantitative analysis of these resonances is achieved, the silicon oxycarbide phase can be described as $SiC_{0.42}O_{1.16}$, which is very close to that determined by elemental analysis. The silicon oxycarbide has the local environments, such as SiC_4, on the basis of our ^{29}Si MAS NMR observation and, therefore, a broad resonance observed at 10−40 ppm in the ^{13}C NMR spectra is attributed to, in part, carbon surrounded by four silicon atoms. In the case of the dipolar dephasing technique, in fact, the 10−40 ppm resonance became slightly intense, relative to other lower-field resonances. Also, as opposed to the general formula, we cannot completely ignore the possibility that the local environment of Si also involves some hydroxyl groups (Si−OH) at present.

As a result of the ESR experiments at various temperatures, the silicon oxycarbide has localized paramagnetic centers, which have been similarly observed for carbon materials.[33] Such paramagnetic centers may be found as unpaired electrons in dangling bonds due to disordered structure of the silicon oxycarbide. The line width change observed in the ESR spectra as measuring temperatures decreased would be related to the mobility in the silicon oxycarbide.

Lithium Species in the Silicon Oxycarbide. It should be repeatedly noted that the structure of silicon oxycarbides relies much on several conditions such as type of precursor, pyrolysis temperature, etc.[23] Therefore, it is understood that our study does not provide a general but rather an example picture of lithium species stored in silicon oxycarbides. Given structural characteristics of the silicon oxycarbide, incumbent carbon materials are considered useful examples to gain insight into the type of lithium species. Graphite has widely been known to store lithium species in a unique manner to form graphite intercalation compounds (GICs).[1] Literature shows that the first-stage structure of GICs has a characteristic resonance at ca. 45 ppm in ^{7}Li NMR spectra.[39,40] Interestingly, on the other hand, nongraphitizable carbon, called hard carbon, shows quite different ^{7}Li NMR resonances from graphite, featuring a dynamic behavior of lithium species upon changing measuring temperatures. This behavior is attributed to the mobility of lithium species stored in at least two sites in hard carbon on the NMR time scale. Lithium species in one site (e.g., microcavity) have been reported to have a more metallic nature, while lithium species in the other site (e.g., between disordered graphitic carbon layers) are thought to have a more ionic nature.[35,36] Another example is carbon materials that are prepared at low temperatures such as 700 °C. This type of carbon usually provides a single resonance at ca. 10 ppm, which does not change in shift even at lower temperatures.[41] The fully lithiated silicon oxycarbide shows a resonance at 3−9 ppm in a wide temperature range (+25 to −120 °C) without any peak separation but rather with only broadening. This behavior monitored in the ^{7}Li NMR spectra is similar to that observed for carbon prepared at low temperatures.[41] If the silicon oxycarbide phase plays a role in structural disordering, it is possible that the silicon oxycarbide mainly stores lithium species in unorganized structures of the free carbon phase. The reversibility of lithium storage in the silicon oxycarbide can be seen in typical electrochemical lithiation and delithiation cycles (Figure 4). Our results show that ionic lithium species are reversibly stored in and released from the silicon oxycarbide. The observed slope voltage curves except the first lithiation suggest that a one-phase reaction occurs in the silicon oxycarbide (Figure 4).[42]

The silicon oxycarbide also has irreversible lithium species that account for ca. 30% of the initial lithiation capacity measured at 0.005 V. In the ^{7}Li NMR spectrum of the silicon oxycarbide lithiated to 0.4 V, the resonance at 0 ppm becomes the main component (67%) when compared to that at 2.4 ppm (33%). If we assume that the 2.4 ppm and the 0 ppm resonance correspond to the 30% reversible and the 70% irreversible lithium species observed between 0.4 and 3 V, respectively, such a contribution of each resonance gives a good agreement by ensuring quantitative accuracy of the ^{7}Li NMR measurements as much as possible. When electrochemical lithiation proceeded further in the silicon oxycarbide, a resonance was shifted to 8.6 ppm. Because the silicon oxycarbide offers much better reversibility of lithiation and delithiation in the range 0.005−0.4 V, it is thought that reversible lithium species have significance with respect to the resonance shift.

Upon delithiation to 3 V, the 0 ppm resonance can also be seen. This result provides a strong indication that the irreversible capacity observed for the silicon oxycarbide is rendered by the formation of some ionic lithium species upon the first lithiation. Previously, it has been reported that ^{7}Li NMR resonances attributed to typical ionic lithium species, such as Li_2O, LiF, and Li_2CO_3, appear in a small shift range +2.8 to −1 ppm relative to LiCl.[43] In the interior and exterior of the silicon oxycarbide, although our measuring condition provides a different resolution due to lower magnetic field when compared to that used in a previous study,[43] these ionic lithium species could be formed. The difference in Li K edge in the EELS spectra shown in Figures 10b and 12b reflects changes in the electronic environment of lithium species. Unfortunately, our EELS analysis does not clearly show any distinct Li K edge in the inner part of the silicon oxycarbide particle, which makes it difficult to indentify lithium species that are not released during delithiation to 1.5 V. If the ionic lithium species evidenced by ^{7}Li NMR analysis after delithiation to 3 V are electrochemically no longer active in subsequent cycles, they should remain completely in the interior and the exterior of the silicon oxycarbide particle. In addition, we see that a fraction of stored lithium species can be reversibly used at >1.5 V, as shown in Figure 4. Thus, both EELS spectra shown in Figures 10b and 12b should also include information on the electronic environment of such reversible lithium species.

It is noticeable that the silicon oxycarbide shows a pseudo-voltage plateau of at least ca. 150 mA h g^{-1} between 0.25 and 0.35 V during the first lithiation but not the second lithiation reaction; the lithiation reaction path at the first cycle is quite different from that at the second cycle (the inset in Figure 4). Generally, the presence of a voltage plateau is an indication of phase transformation.[42] It has been reported that transition metal oxides (metal = Fe or Co, for example) can reversibly store and release lithium by forming metallic nanoparticles in a Li_2O matrix and that the size of the nanoparticles becomes a key factor of reversible Li_2O formation and decomposition.[44] This transformation gives a different lithiation curve compared to that observed at subsequent cycles. The nanosized characteristics apparently remain in the active materials once formed at the first lithiation. Li et al. also reported the theoretical electromotive force value (0.694 V) for the reaction of bulk SiO_2 and Li based on the Nernst equation.[45] Our ^{29}Si MAS NMR analysis shows that the silicon oxycarbide includes

the SiO_4 unit in the glass network, which makes up almost 50% of the total amount of oxygen. The SiO_4 unit might fully react with lithium to form Li_2O in a way similar to that discussed for transition metal oxides.[45] However, the silicon oxycarbide has at least four different Si units and the free carbon phase. Even assuming that such a reaction occurs in the silicon oxycarbide, it would be a more complicated structural reorganization process involving bond breaking and formation. The paramagnetic centers found in the silicon oxycarbide might partly be associated with the lithiation reaction as proposed for carbon materials.[46,47] Given the spin density of the silicon oxycarbide, however, the paramagnetic centers appear to contribute far less to the observed irreversible capacity of 297 mA h g^{-1} (=1159 − 862 mA h g^{-1}).

On the surface of the silicon oxycarbide, it would be reasonable to suppose that the SEI layer forms via decomposition of the electrolyte, as usually seen in the case of anode materials.[25] This SEI formation is partly involved in the initial reaction that consumes irreversibly charges. It is known that the composition of SEI varies depending on type of electrolyte.[48] When the $LiPF_6$ salt is used in the electrolyte, LiF has been reported to be a major component of SEI, as detected by X-ray photoelectron spectroscopy analysis, on graphite.[27] It may be difficult to clearly distinguish the Li K edge between $LiPF_6$ and LiF in the EELS spectra.[49] Because the electrodes used were washed prior to a series of analyses, however, the residual electrolyte should contribute little, if any, to our measurements. As indicated by both EELS and EDX measurements, LiF appears to be the only identified compound present near the surface of the silicon oxycarbide particle particularly after 28 cycles (points 16 and 20 in Figure 12b). It is also possible that some O- and P-containing compounds, such as Li_xPOF_y species, form on the surface via decomposition of the $LiPF_6$ salt.[48,50] The thickness of the SEI layer including LiF and O- and P-containing compounds appears to vary depending on location of the surfaces. This variation could happen given the perception that the nature of the SEI layer is very sensitive to small changes in surface condition.

There is uncertainty that the SEI layer is damaged by radiation, which inhibits observation of the electronic environment of Li in its pristine form. As reported previously,[49] if radiation damage occurs, LiF could transform into Li_2O due to the presence of residual oxygen and/or moisture in the equipment. In this regard, we believe that our analytical condition suppresses such possible radiation damage without affecting interpretations.

According to the difference between the electrodes after 2 and 28 cycles in the STEM/EDX results, the thickness of the SEI layer including LiF and O- and P-containing compounds is likely to grow over electrochemical cycling. Similar phenomena have been reported for anode materials, leading to an increase in internal resistance.[48] Likewise, the SEI layer growth can be partly responsible for a descending trend in lithiation and delithiation capacity toward 28 cycles for the silicon oxycarbide. To suppress the SEI layer growth on the silicon oxycarbide particles, careful choice of the electrolyte may be necessary as well as concurrent use of additives such as vinylidene carbonate.[25]

CONCLUSION

There has not yet been a full understanding of the electrochemically lithiated and delithiated states of silicon oxycarbides. In the present work, attention has been directed to lithium species accommodated by a representative silicon oxycarbide prepared from a cured form of poly(methylhydrogensiloxane) and divinylbenzene. The chemical composition of the silicon oxycarbide was determined to be $SiO_{1.2}C_{3.7}H_{0.8}$. Several analytical methods have shown that the silicon oxycarbide has excess free carbon other than carbon bound to silicon. ^{7}Li NMR analysis confirms that lithium species have ionic natures in both fully lithiated and fully delithiated silicon oxycarbides. Even at −120 °C, the fully lithiated silicon oxycarbide does not show any peak separation but broadening within a narrow range of resonance shift. These results give an idea that such ionic lithium species are not involved in any dynamic exchange between greatly differing sites on the NMR time scale. A majority of the ionic lithium species (ca. 70%) stored to 0.4 V with respect to lithium is apparently related to the first-cycle irreversibility, whereas better reversibility of lithiation and delithiation is found in the range 0.005−0.4 V. The Li K edge in EELS can be generally used as a valuable source to verify the electronic environment of lithium species. Indistinct Li K edge spectra inhibit the identification of ionic lithium species in the interior of the delithiated silicon oxycarbide in this study. However, LiF and O- and P-containing compounds detected by EELS and EDX mapping appear to be major components in the SEI layer, which tends to become thick over repeated lithiation and delithiation. These compounds are thought to cause part of the initial irreversible capacity and capacity fading over electrochemical cycling.

ASSOCIATED CONTENT

Supporting Information

HAADF-STEM image and EDX (C, O, and Si) mapping images of the silicon oxycarbide embedded in an epoxy resin, EELS C K edge, O K edge, and Si L edge spectra of the delithiated working electrode after 2 and 28 cycles. This material is available free of charge via the Internet at http://pubs.acs.org.

AUTHOR INFORMATION

Corresponding Author

*Hiroshi Fukui. Fax: +81-465-76-3101. Tel: +81-465-75-1064. E-mail: h.fukui@dowcorning.com.

Notes

The authors declare no competing financial interest.

ACKNOWLEDGMENTS

The authors are grateful to Dow Corning Corporation and Dow Corning Toray Co. Ltd. for financial support of this work.

REFERENCES

(1) Ohzuku, T.; Iwakoshi, Y.; Sawai, K. Formation of Lithium-Graphite Intercalation Compounds in Nonaqueous Electrolytes and Their Application as a Negative Electrode for a Lithium Ion (Shuttlecock) Cell. *J. Electrochem. Soc.* **1993**, *140*, 2490−2498.

(2) Obrovac, M. N.; Krause, L. J. Reversible Cycling of Crystalline Silicon Powder. *J. Electrochem. Soc.* **2007**, *154*, A103−A108.

(3) Liu, N.; Wu, H.; McDowell, M. T.; Yao, Y.; Wang, C.; Cui, Y. A Yolk-Shell Design for Stabilized and Scalable Li-Ion Battery Alloy Anodes. *Nano Lett.* **2012**, *12*, 3315−3321.

(4) Chen, X.; Li, X.; Ding, F.; Xu, W.; Xiao, J.; Cao, Y.; Meduri, P.; Liu, J.; Graff, G. L.; Zhang, J.-G. Conductive Rigid Skeleton Supported Silicon as High-Performance Li-Ion Battery Anodes. *Nano Lett.* **2012**, *12*, 4124−4130.

(5) Wu, H.; Zheng, G.; Liu, N.; Carney, T. J.; Yang, Y.; Cui, Y. Engineering Empty Space between Si Nanoparticles for Lithium-Ion Battery Anodes. *Nano Lett.* **2012**, *12*, 904−909.
(6) Konno, H.; Kasashima, T.; Azumi, K. Application of Si−C−O Glass-like Compounds as Negative Electrode Materials for Lithium Hybrid Capacitors. *J. Power Sources* **2009**, *191*, 623−627.
(7) Shen, J.; Ahn, D.; Raj, R. C-Rate Performance of Silicon Oxycarbide Anodes for Li^+ Batteries Enhanced by Carbon Nanotubes. *J. Power Sources* **2011**, *196*, 2875−2878.
(8) Sanchez-Jimenez, P. E.; Raj, R. Lithium Insertion in Polymer-Derived Silicon Oxycarbide Ceramics. *J. Am. Ceram. Soc.* **2010**, *93*, 1127−1135.
(9) Fukui, H.; Ohsuka, H.; Hino, T.; Kanamura, K. A Si−O−C Composite Anode: High Capability and Proposed Mechanism of Lithium Storage Associated with Microstructural Characteristics. *ACS Appl. Mater. Interfaces* **2010**, *2*, 998−1008.
(10) Fukui, H.; Nakata, N.; Dokko, K.; Takemura, B.; Ohsuka, H.; Hino, T.; Kanamura, K. Lithiation and Delithiation of Silicon Oxycarbide Single Particles with a Unique Microstructure. *ACS Appl. Mater. Interfaces* **2011**, *3*, 2318−2322.
(11) Bhandavat, R.; Singh, G. Stable and Efficient Li-Ion Battery Anodes Prepared from Polymer-Derived Silicon Oxycarbide−Carbon Nanotube Shell/Core Composites. *J. Phys. Chem. C* **2013**, *117*, 11899−11905.
(12) Liu, X.; Xie, K.; Wang, J.; Zheng, C.; Pan, Y. Si/Si−O−C Composite Anode Materials Exhibiting Good C Rate Performances Prepared by a Sol−Gel Method. *J. Mater. Chem.* **2012**, *22*, 19621−19624.
(13) Liu, X.; Zheng, M.-C.; Xie, K.; Liu, J. The Relationship between the Electrochemical Performance and the Composition of Si−O−C Materials Prepared from a Phenyl-Substituted Polysiloxane Utilizing Various Processing Methods. *Electrochim. Acta* **2012**, *59*, 304−309.
(14) Dibandjo, P.; Graczyk-Zajac, M.; Riedel, R.; Pradeep, V. S.; Soraru, G. D. Lithium Insertion into Dense and Porous Carbon-Rich Polymer-Derived SiOC Ceramics. *J. Eur. Ceram. Soc.* **2012**, *32*, 2495−2503.
(15) Graczyk-Zajac, M.; Toma, L.; Fasel, C.; Riedel, R. Carbon-Rich SiOC Anodes for Lithium-Ion Batteries: Part I. Influence of Material UV-Pre-Treatment on High Power Properties. *Solid State Ionics* **2012**, *225*, 522−526.
(16) Kaspar, J.; Graczyk-Zajac, M.; Riedel, R. Carbon-Rich SiOC Anodes for Lithium-Ion Batteries: Part II. Role of Thermal Cross-Linking. *Solid State Ionics* **2012**, *225*, 527−531.
(17) Kaspar, J.; Graczyk-Zajac, M.; Riedel, R. Determination of the Chemical Diffusion Coefficient of Li-Ions in Carbon-Rich Silicon Oxycarbide Anodes by Electro-Analytical Methods. *Electrochim. Acta* **2014**, *115*, 665−670.
(18) Fukui, H.; Ohsuka, H.; Hino, T.; Kanamura, K. Silicon Oxycarbides in Hard-Carbon Microstructures and Their Electrochemical Lithium Storage. *J. Electrochem. Soc.* **2013**, *160*, A1276−A1281.
(19) Kaspar, J.; Graczyk-Zajac, M.; Riedel, R. Lithium Insertion into Carbon-Rich SiOC Ceramics: Influence of Pyrolysis Temperature on Electrochemical Properties. *J. Power Sources* **2013**, *244*, 450−455.
(20) Fukui, H.; Eguchi, K.; Ohsuka, H.; Hino, T.; Kanamura, K. Structures and Lithium Storage Performance of Si−O−C Composite Materials Depending on Pyrolysis Temperatures. *J. Power Sources* **2013**, *243*, 152−158.
(21) Liu, X.; Zheng, M.-C.; Xie, K. Mechanism of Lithium Storage in Si−O−C Composite Anodes. *J. Power Sources* **2011**, *196*, 10667−10672.
(22) Pradeep, V. S.; Graczyk-Zajac, M.; Riedel, R.; Soraru, G. D. New Insights into the Lithium Storage Mechanism in Polymer Derived SiOC Anode Materials. *Electrochim. Acta* **2014**, *119*, 78−85.
(23) Mutin, P. H. Control of the Composition and Structure of Silicon Oxycarbide and Oxynitride Glasses Derived from Polysiloxane Precursors. *J. Sol-Gel Sci. Technol.* **1999**, *14*, 27−38.
(24) Bréquel, H.; Parmentier, J.; Walter, S.; Badheka, R.; Trimmel, G.; Masse, S.; Latournerie, J.; Dempsey, P.; Turquat, C.; Desmartin-Chomel, A.; Le Neindre-Prum, L.; Jayasooriya, U. A.; Hourlier, D.; Kleebe, H.-J.; Sorarù, G. D.; Enzo, S.; Babonneau, F. Systematic Structural Characterization of the High-Temperature Behavior of Nearly Stoichiometric Silicon Oxycarbide Glasses. *Chem. Mater.* **2004**, *16*, 2585−2598.
(25) Xu, K. Nonaqueous Liquid Electrolytes for Lithium-Based Rechargeable Batteries. *Chem. Rev.* **2004**, *104*, 4303−4418.
(26) Kanamura, K.; Shiraishi, S.; Takezawa, H.; Takehara, Z. XPS Analysis of the Surface of a Carbon Electrode Intercalated by Lithium Ions. *Chem. Mater.* **1997**, *9*, 1797−1804.
(27) Leroy, S.; Martinez, H.; Dedryvère, R.; Lemordant, D.; Gonbeau, D. Influence of the Lithium Salt Nature over the Surface Film Formation on a Graphite Electrode in Li-Ion Batteries: An XPS Study. *Appl. Surf. Sci.* **2007**, *253*, 4895−4905.
(28) Hatcher, P. G. Chemical Structural Studies of Natural Lignin by Dipolar Dephasing Solid-State ^{13}C Nuclear Magnetic Resonance. *Org. Geochem.* **1987**, *11*, 31−39.
(29) Taylor, R. B.; Parbhoo, B.; Fillmore, D. M. In *The Analytical Chemistry of Silicones*; Smith, A. L., Ed.; Wiley-Interscience: New York, 1991; pp 347−419.
(30) Widgeon, S. J.; Sen, S.; Mera, G.; Ionescu, E.; Riedel, R.; Navrotsky, A. ^{29}Si and ^{13}C Solid-State NMR Spectroscopic Study of Nanometer-Scale Structure and Mass Fractal Characteristics of Amorphous Polymer Derived Silicon Oxycarbide Ceramics. *Chem. Mater.* **2010**, *22*, 6221−6228.
(31) Cheng, H. N.; Wartelle, L. H.; Klasson, K. T.; Edwards, J. C. Solid-State NMR and ESR Studies of Activated Carbons Produced from Pecan Shells. *Carbon* **2010**, *48*, 2455−2469.
(32) Pradeep, V. S.; Graczyk-Zajac, M.; Wilamowska, M.; Riedel, R.; Soraru, G. D. Influence of Pyrolysis Atmosphere on the Lithium Storage Properties of Carbon-Rich Polymer Derived SiOC Ceramic Anodes. *Solid State Ionics* **2014**, *262*, 22−24.
(33) Alcántara, R.; Ortiz, G. F.; Lavela, P.; Tirado, J. L.; Stoyanova, R.; Zhecheva, E. EPR, NMR, and Electrochemical Studies of Surface-Modified Carbon Microbeads. *Chem. Mater.* **2006**, *18*, 2293−2301.
(34) Ahn, D.; Raj, R. Thermodynamic Measurements Pertaining to the Hysteretic Intercalation of Lithium in Polymer-Derived Silicon Oxycarbide. *J. Power Sources* **2010**, *195*, 3900−3906.
(35) Tatsumi, K.; Conard, J.; Nakahara, M.; Menu, S.; Lauginie, P.; Sawada, Y.; Ogumi, Z. ^7Li NMR Studies on a Lithiated Non-Graphitizable Carbon Fibre at Low Temperatures. *Chem. Commun.* **1997**, 687−688.
(36) Guérin, K.; Ménétrier, M.; Février-Bouvier, A.; Flandrois, S.; Simon, B.; Biensan, P. A Li NMR Study of a Hard Carbon for Lithium−Ion Rechargeable Batteries. *Solid State Ionics* **2000**, *127*, 187−198.
(37) Sato, T.; Morikawa, A.; Suzuki, Y.; Iwahori, T. Air Protection System for Structural Analysis of High Active Materials. *Kenbikyo* **2011**, *46*, 266−269.
(38) Liu, G.; Kaspar, J.; Reinold, L. M.; Graczyk-Zajac, M.; Riedel, R. Electrochemical Performance of DVB-Modified SiOC and SiCN Polymer-Derived Negative Electrodes for Lithium-Ion Batteries. *Electrochim. Acta* **2013**, *106*, 101−108.
(39) Tatsumi, K.; Akai, T.; Imamura, T.; Zaghib, K.; Iwashita, N.; Higuchi, S.; Sawada, Y. ^7Li-Nuclear Magnetic Resonance Observation of Lithium Insertion into Mesocarbon Microbeads. *J. Electrochem. Soc.* **1996**, *143*, 1923−1930.
(40) Letellier, M.; Chevallier, F.; Béguin, F. In situ ^7Li NMR during Lithium Electrochemical Insertion into Graphite and a Carbon/Carbon Composite. *J. Phys. Chem. Solids* **2006**, *67*, 1228−1232.
(41) Tatsumi, K.; Conard, J.; Nakahara, M.; Menu, S.; Lauginie, P.; Sawada, Y.; Ogumi, Z. Low Temperature ^7Li-NMR Investigations on Lithium Inserted into Carbon Anodes for Rechargeable Lithium-Ion Cells. *J. Power Sources* **1999**, *81*−*82*, 397−400.
(42) Winter, M.; Brodd, R. J. What Are Batteries, Fuel Cells, and Supercapacitors? *Chem. Rev.* **2004**, *104*, 4245−4270.
(43) Meyer, B. M.; Leifer, N.; Sakamoto, S.; Greenbaum, S. G.; Grey, C. P. High Field Multinuclear NMR Investigation of the SEI Layer in

Lithium Rechargeable Batteries. *Electrochem. Solid-State Lett.* **2005**, *8*, A145−A148.
(44) Poizot, P.; Laruelle, S.; Grugeon, S.; Dupont, L.; Tarascon, J.-M. Nano-Sized Transition-Metal Oxides as Negative-Electrode Materials for Lithium-Ion Batteries. *Nature* **2000**, *407*, 496−499.
(45) Li, H.; Balaya, P.; Maier, J. Li-Storage via Heterogeneous Reaction in Selected Binary Metal Fluorides and Oxides. *J. Electrochem. Soc.* **2004**, *151*, A1878−A1885.
(46) Menachem, C.; Wang, Y.; Flowers, J.; Peled, E.; Greenbaum, S. G. Characterization of Lithiated Natural Graphite before and after Mild Oxidation. *J. Power Sources* **1998**, *76*, 180−185.
(47) Matsumura, Y.; Wang, S.; Mondori, J. Mechanism Leading to Irreversible Capacity Loss in Li Ion Rechargeable Batteries. *J. Electrochem. Soc.* **1995**, *142*, 2914−2918.
(48) Etacheri, V.; Haik, O.; Goffer, Y.; Roberts, G. A.; Stefan, I. C.; Fasching, R.; Aurbach, D. Effect of Fluoroethylene Carbonate (FEC) on the Performance and Surface Chemistry of Si-Nanowire Li-Ion Battery Anodes. *Langmuir* **2012**, *28*, 965−976.
(49) Wang, F.; Graetz, J.; Moreno, M. S.; Ma, C.; Wu, L.; Volkov, V.; Zhu, Y. Chemical Distribution and Bonding of Lithium in Intercalated Graphite: Identification with Optimized Electron Energy Loss Spectroscopy. *ACS Nano* **2011**, *5*, 1190−1197.
(50) Eriksson, T.; Andersson, A. M.; Gejke, C.; Gustafsson, T.; Thomas, J. O. Influence of Temperature on the Interface Chemistry of $Li_xMn_2O_4$ Electrodes. *Langmuir* **2002**, *18*, 3609−3619.